



Contents lists available at ScienceDirect

Arabian Journal of Chemistry

journal homepage: www.ksu.edu.sa

Effects of hydroxyapatite content on cytotoxicity, bioactivity and strength of metakaolin/hydroxyapatite composites

Nattaphon Twinprai^a, Ratchawoot Sutthi^b, Piboon Ngaonee^c, Patamaporn Chaikool^d, Tularat Sookto^e, Prin Twinprai^f, Yoshiharu Mutoh^g, Prinya Chindaprasirt^{h,i}, Teerawat Laonapakul^{j,*}

^a Trauma Unit, Department of Orthopedics, Srinagarind Hospital, Faculty of Medicine, Khon Kaen University, Khon Kaen, 40002, Thailand

^b Department of Industrial Engineering and Logistics Program, Faculty of Arts and Science, Chaiyaphum Rajabhat University, Chaiyaphum, 36000, Thailand

^c Division of Cytogenetics Research, Faculty of Dentistry, Khon Kaen University, Khon Kaen, 40002, Thailand

^d Department of Mechanical Engineering, Faculty of Engineering, Rajamangala University of Technology Isan Khon Kaen Campus, Khon Kaen, 40000, Thailand

^e Department of Prosthetic Dentistry, Faculty of Dentistry, Khon Kaen University, Khon Kaen, 40002, Thailand

^f Musculoskeletal Unit, Department of Radiology, Srinagarind Hospital, Khon Kaen University, Khon Kaen, 40002, Thailand

^g Professor Emeritus Nagaoka University of Technology, Nagaoka, Niigata 940-2188, Japan

^h Sustainable Infrastructure Research and Development Center, Department of Civil Engineering, Faculty of Engineering, Khon Kaen University, Khon Kaen, 40002, Thailand

ⁱ Academy of Science, Royal Society of Thailand, Dusit, Bangkok, 10300, Thailand

^j Department of Industrial Engineering, Faculty of Engineering, Khon Kaen University, Khon Kaen, 40002, Thailand

ARTICLE INFO

Keywords:

Cell viability
Apatite formation
Compressive strength
Geopolymer composite
Bone substitute material

ABSTRACT

The development of new materials is a critical challenge in advancing bone repair technology. Nowadays, the use of high strength geopolymers is extended to various fields, including biomedical research. This study investigates the influence of hydroxyapatite (HAp) content on the *in vitro* properties and characteristics of the metakaolin/HAp (MK/HAp) composites for potential application as bone substitutes. The MK/HAp composites with varying HAp contents were fabricated and subjected to cytotoxicity, bioactivity, physical and mechanical testing. PrestoBlue assay results confirmed acceptable osteoblast cell compatibility for all composites, with cell viability increases with increasing HAp content. Simulated body fluid (SBF) immersion demonstrated enhanced bioactivity and bone-like apatite formation on the composite surfaces with increasing HAp content. The compressive strength of the composite decreased mainly due to the reduced amount of silica and alumina contents and the increased porosity with higher HAp. Based on the present results, the relationship between bioactivity and strength with variations in HAp content indicates a promising composite. The HAp content of the MK/HAp composites for a bone substitute material should be 50% or higher to match the apatite formation and strength of specific human bones.

1. Introduction

Bone tissue disease and damage that can occur in various parts of the human body, such as wrist, hip and spine fractures, affect 30–40 % of the population in developed countries (Kanis, 2007). Cancellous bone, primarily composed of trabecular bone tissue, is a type of autologous bone graft. Compared to cortical bone grafts, cancellous bone grafts exhibit relatively high osteogenic and osteoinductive properties (Herford et al., 2014). Hydroxyapatite (HAp, $\text{Ca}_{10}(\text{PO}_4)_6(\text{OH})_2$) is widely used for bone substitution applications due to its excellent biocompatibility and

bioactivity (osteoconduction and osteoinduction) (Kim et al., 2022). However, one of the biggest problems in its use as a bone substitute material is its poor mechanical strength. The compressive strengths of cancellous and trabecular human bones are not high in the range of 2–15 MPa and those of HAp are 2–7.1 MPa (Sakka et al., 2013; Metzner et al., 2021; Misch et al., 1999; Jurgelane et al., 2021; Alvarado et al., 2023). Although the fully dense HAp compressive strength is higher (Brown, 2001). The 2–7.1 MPa range we used in the literature reflects the compressive strength of HAp prepared by the sintering methods similar to the approach used in our study. This low strength of HAp bulk

* Corresponding author at: Department of Industrial Engineering, Faculty of Engineering, Khon Kaen University, Khon Kaen, 40002, Thailand.
E-mail address: teerla@kku.ac.th (T. Laonapakul).

<https://doi.org/10.1016/j.arabjc.2024.105878>

Received 2 April 2024; Accepted 13 June 2024

Available online 15 June 2024

1878-5352/© 2024 The Author(s). Published by Elsevier B.V. on behalf of King Saud University. This is an open access article under the CC BY-NC-ND license (<http://creativecommons.org/licenses/by-nc-nd/4.0/>).

materials restricts their utilization in load-bearing applications. Hydroxyapatite composites are widely used to enhance the mechanical strength of implants for load-bearing applications (Shuai et al., 2022). However, for bone substitute materials, achieving a balance between mechanical properties and biological properties is crucial. Additionally, an appropriate porosity is essential for cell migration, adhesion, tissue formation, and nutrient diffusion within the scaffold (Shuai et al., 2021; Feng et al., 2023).

Geopolymers are candidates for bone substitute materials owing to their high strength. They are fabricated by converting aluminosilicate raw materials, such as clay and fly ash, into a covalently linked 3D network comprised of $[-Si-O-Al-O-]_n$ bonds of geopolymers using an alkaline activator solution (Wang et al., 2019). Kaolin or China clay is a clay-like material that is rich in kaolinite. Kaolinite is the most common clay mineral used for geopolymer fabrication. Currently, geopolymers made from kaolin have been applied in various fields, such as insulating construction materials (Matakhah et al., 2023), fire resistant materials (Lahoti et al., 2019), and adsorption materials (Du et al., 2022). Furthermore, the applicability of kaolinite in regenerative dentistry has been studied by Müller et al. (2020). The results indicate that kaolinite has no toxicity, but further modification for successful application in regenerative dentistry is required. However, the applications of geopolymers as bone substitute materials are currently limited, despite their advantageous properties, including high strength, rapid solidification, and color. Obada et al. (2021) studied the utilization of kaolin to modify the properties of compacted hydroxyapatite scaffolds using a sol-gel technique for bone tissue engineering. Their results showed that kaolin reinforced hydroxyapatite with 15 % of kaolin content enhanced compressive strength to between 5.67 and 7.66 MPa with superior biocompatibility and bioactivity in scaffolds.

Metakaolin can be produced by heating kaolinite clay to temperatures between 600 and 800 °C. Metakaolin powder produced by crushing calcined kaolin is used as a source material for fabricating a geopolymer and its composites (Maruoka et al., 2023; Moya et al., 2024). The compressive strengths of metakaolin geopolymers have been reported to be in the range of 21.2 to 33.3 MPa (Maruoka et al., 2023) and their bioactivity has been confirmed by observing apatite formation on geopolymer surfaces after immersion in a simulated body fluid for 21 days (Catauro et al., 2014). Although some works on the application of metakaolin in biomedical materials have been done, it is still desirable to improve the bioactivity of the metakaolin geopolymer. One of the possible ways to do this is HAP addition into the metakaolin geopolymer to form a metakaolin/HAP composite. de Andrade et al. (2023) conducted a study on the structure, mechanical properties, and biocompatibility of metakaolin-based hydroxyapatite composites (HAP 15 wt% metakaolin geopolymer) on a polyurethane template. The composites demonstrated non-toxicity and their compressive strengths ranged from 1.18 to 2.9 MPa. Our previous work (Sutthi et al., 2018) showed that the compressive strengths ranged from 36.5 to 37.5 MPa for a 25 wt% HAP metakaolin/hydroxyapatite composite. Although the compressive strength and bioactivity of metakaolin/HAP composites have been investigated in previous studies, details of mechanisms for variation of bioactivity and strength with HAP addition are not yet fully understood. Furthermore, the effects of the HAP content on compressive strength, grade of cytotoxicity and bioactivity for the metakaolin/HAP composites have not yet been clarified. Understanding the effects of HAP content is important for considering its proper content in metakaolin/HAP composites. This is because there is a competitive relationship between improvement in strength and bioactivity due to variations of HAP content in metakaolin/HAP composites.

Therefore, in the present study, metakaolin and metakaolin/HAP composites with a wide range of HAP contents were fabricated to investigate the effects of HAP content on density, porosity, cytotoxicity, bioactivity and compressive strength.

2. Materials and characterization procedures

2.1. Material and sample preparation

The metakaolin was prepared by calcinating kaolin clay powder in an electric furnace at 600 °C for 3 h. This clay was collected from Ranong province in southern Thailand. The HAP was prepared using a mechanical process combined with a solid-state reaction of $CaCO_3$ from golden apple snail shells and dibasic calcium phosphate dihydrate ($CaHPO_4 \cdot 2H_2O$, DCPD) (≥ 98 %, Sigma-Aldrich, USA) (Laonapakul et al., 2021). Metakaolin (MK) and HAP were separately crushed into powders, then passed through a 100-mesh screen and stored in a desiccator. Chemical compositions of MK and HAP powders measured using X-ray fluorescence (WDXRF, AXios mAX) are shown in Tables 1 and 2, respectively.

Sodium hydroxide (NaOH, 10 M, AGC Chemicals, Thailand) and sodium silicate (Na_2SiO_3 , 15.3 % Na_2O , 32.8 % SiO_2 , and 51.8 % H_2O , Eastern Silicate, Thailand) with a weight ratio of 1.0 were used as a liquid activated binder (alkali activator solution) for producing metakaolin bulk and metakaolin/HAP composites (Pangdaeng et al., 2018). The alkaline solution weight includes the mass of water. The paste samples were prepared by mixing pure metakaolin (MK1.0) and metakaolin/HAP (MK/HAP) powders with weight ratios of 3/1 (MK0.75H), 1/1 (MK0.5H), and 1/3 (MK0.25H) in a planetary mixer for 15 min. The activator solution was then added and mixing was continued for another 5 min. The weight ratio of mixed powder to activator solution for preparing paste samples was 1:1 (Sutthi et al., 2018; Pangdaeng et al., 2018).

For *in vitro* cytotoxicity and bioactivity determination, paste samples were poured into round acrylic tablet moulds (2 mm thick and 10 mm diameter). Paste samples were poured into $25 \times 25 \times 25$ mm cubic moulds for preparing physical and mechanical test specimens. The moulded paste samples were vibrated for 15 s to eliminate entrapped air and wrapped with cling film to prevent moisture loss. After storing at room temperature for 1 h, the moulded samples were then cured in an electric oven at 80 °C for 14 days (Sutthi et al., 2018). After curing, the samples were demoulded (denoted as post-cured samples) and stored in a desiccator.

2.2. Material characterization

2.2.1. Density and porosity tests

Bulk density, apparent density, percentage of apparent porosity and water absorption of the post-cured samples were determined using the cube samples in accordance with ASTM standard (ASTM C373-88, 2006). The dried mass (D) was determined using the post-cured cube samples, which were dried in an oven at 110 °C for 24 h, and then left to cool in a desiccator. The mass of a boiled sample suspended in water (S) was measured using the dried samples, which were boiled in distilled water for 5 h and cooled in water for 24 h. Saturated mass (M) was measured using the boiled samples after their surfaces were wiped using a dry towel. Their bulk density, apparent density, percentage of apparent porosity and water absorption were estimated as:

$$\text{Bulk density (g/cm}^3\text{)} = \frac{D}{(M - S)} \times \rho W : \rho W = 1 \text{ g/cm}^3 \quad (1)$$

$$\text{Apparent density (g/cm}^3\text{)} = \frac{D}{(D - S)} \times \rho W : \rho W = 1 \text{ g/cm}^3 \quad (2)$$

$$\begin{aligned} \text{Percentage of apparent porosity (\%)} &= \left(1 - \frac{\text{Bulk density}}{\text{Apparent density}}\right) \times 100 \\ &= \frac{(M - D)}{(M - S)} \times 100 \quad (3) \end{aligned}$$

Table 1
Chemical composition of MK powder.

Chemical composition	SiO ₂	Al ₂ O ₃	TiO ₂	Fe ₂ O ₃	K ₂ O	P ₂ O ₅	CaO	MgO	SO ₃	LOI*
wt %	59.58	35.71	1.03	1.06	0.89	0.83	0.15	0.17	0.03	0.55

* LOI = loss on ignition

Table 2
Chemical composition of HAp powder.

Chemical composition	CaO	P ₂ O ₅	MgO	Na ₂ O	Al ₂ O ₃	SiO ₂	Cl	SO ₃	MnO	LOI*
wt %	53.19	42.72	1.22	0.96	0.58	0.20	0.14	0.07	0.04	0.88

* LOI = loss on ignition

$$\text{Percentage of water absorption (\%)} = \frac{(M - D)}{D} \times 100 \quad (4)$$

In the present study, results are reported as the average values of five sample measurements.

2.2.2. Cytotoxicity assay

2.2.2.1. Cell culture. A human normal osteoblast cell line, hFOB 1.19 (ATCC, CRL11372), was purchased from the ATCC (Biomedica, a distributor of ATCC). The osteoblast cells were cultured in Dulbecco's Modified Eagle's Medium with no phenol red (DMEM, no phenol red, Gibco) supplemented with 10 % fetal bovine serum (FBS, Gibco) and 300 µg/ml of a selective antibiotic (Geneticin (G418, Gibco)). The medium was changed every 3 days. Experiments were done at 37 °C in a humidified atmosphere of 5 % CO₂ and 95 % air. When nearing confluency, cells were subcultured using trypsin/EDTA (0.25 %, Gibco) and inoculated into new flasks with a split ratio of 1:3. The cells were cultured until reaching 80 % confluency for cell viability testing.

2.2.2.2. Cell viability assay. *In vitro* cytotoxicity of the samples was evaluated using a PrestoBlue assay. The cells were seeded at a density of 50,000 cells/well in 12-well plates with 1.5 mL of the culture medium per well, and then incubated at 37 °C with 5 % CO₂. After 24 h of incubation, 1.0 mL of culture medium was refreshed in each well. Transwell inserts were loaded with different weights (30 and 90 g) of the post-cured samples (MK1.0, MK0.75H, MK0.5H and MK0.25H) and added to the cells. Culture medium with no sample was used as a positive control, and 10 % dimethyl sulfoxide (DMSO, Merck) in culture medium was used as a negative control. Each test was done in triplicate. Culture plates were assayed 24 h after sample addition. A PrestoBlue assay was used in this study to measure cell viability. After 24 h of treatment, the culture medium was removed and replaced with PrestoBlue reagent (diluted 10-fold in culture medium; 300 µL/well, Thermo Fisher Scientific), followed by further incubation for 45 min to assess cell viability. Finally, cell viability was analyzed by measuring the fluorescent absorbance signal using a Varioskan LUX Multimode Microplate Reader (Thermo Scientific) at wavelengths of 560 nm (excitation) and 590 nm (emission). The obtained fluorescence readings were used to calculate cell viability as follows:

$$\% \text{Cell viability} = A_S/A_C \times 100 \quad (5)$$

where A_S and A_C represent the average absorbance values of a sample well and of the positive control well, respectively.

2.2.3. *In vitro* bioactivity test and sample characterizations

SBF, which has an ionic concentration comparable to that of human blood plasma, was prepared using the method of Kokubo and Takadama (2006). Post-cured tablet samples were immersed in SBF for 3, 7, 14 and 28 days to investigate the influence of an *in vitro* environment on precipitation of bone-like apatite. The temperature of the SBF was kept

constant at 37 ± 0.2 °C (human body temperature) during immersion. For morphological observation, the samples were sputter-coated with gold at an appropriate voltage. The surface morphologies of the tablet samples were studied using scanning electron microscopy (SEM/EDS, Zeiss LEO Model 1450, with a secondary electron detector) before and after immersion in the SBF to verify calcium phosphate apatite precipitation. An EDS with acceleration voltage of 20 keV was used to determine the elemental composition of sample surfaces. The calcium/phosphorus (Ca/P) molar ratio was calculated from the resultant elemental composition of the sample surface by averaging five measurements. The EDS findings were cross-referenced using X-ray diffraction (XRD) analysis. The crystalline phases of the samples were identified using X-ray diffractometry (XRD, Bruker D8), with CuKα radiation at 40 kV and 40 mA with a scan rate of 2.4° 2θ/min in 0.02° 2θ increments.

Compressive strength tests of cube samples were performed in accordance with ASTM C109/C109M-21 (ASTM C109/C109M, 2021) using hydraulic testing equipment with a maximum load of 400 kN. Compressive strength testing of the samples was conducted at a loading rate of 2 kN/s. The compressive strengths were measured for the post-cured and dried samples after immersion in SBF for 28 days. Compressive strength values are reported as the average value of five measurements.

3. Results and discussion

3.1. Density, porosity and crystalline structure of the samples

The appearances of the post-cured samples (MK1.0, MK0.75H, MK0.5H and MK0.25H) are shown in Fig. 1. Specimens at all mixing weight ratios were successfully compacted into both cubic and tablet shapes.

The relationships between bulk, apparent densities and percentage of HAp content are shown in Fig. 2(a). Conceptually, only impermeable pores of the sample comprise the sample volume for apparent density. However, the volume corresponding to bulk density also includes capillary and voids generated during packing in addition to the impermeable pores. In Fig. 2(a), the bulk density of the samples decreased with increasing HAp content, from 1.89 to 1.14 g/cm³. In contrast, the apparent density of the samples increased with HAp content. These results suggest that an increased HAp content enhances the total internal porosity of the sample. The reason for the greater porosity with increasing HAp content is as follows. Geopolymerization takes place primarily between the alkaline solution and the alumino-silicate source (metakaolin), while the HAp does not react with the alkaline solution. The unreacted HAp powder and its agglomerates would disrupt the packing of the metakaolin matrix. This can lead to the formation of capillaries, pores, and voids, decreasing the bulk density while increasing the apparent density of the composite. Additionally, the unreacted HAp may leave a residue of alkaline solution remaining from the reaction with MK. The release of residual alkaline solutions could

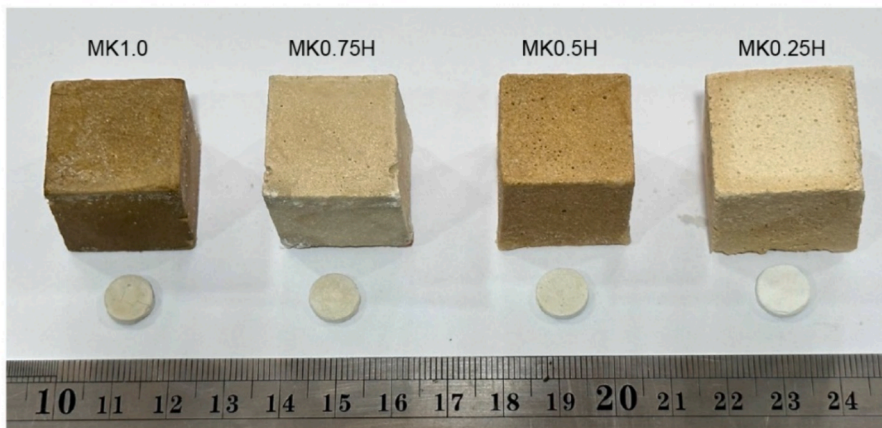


Fig. 1. Post-cured samples (MK1.0, MK0.75H, MK0.5H and MK0.25H).

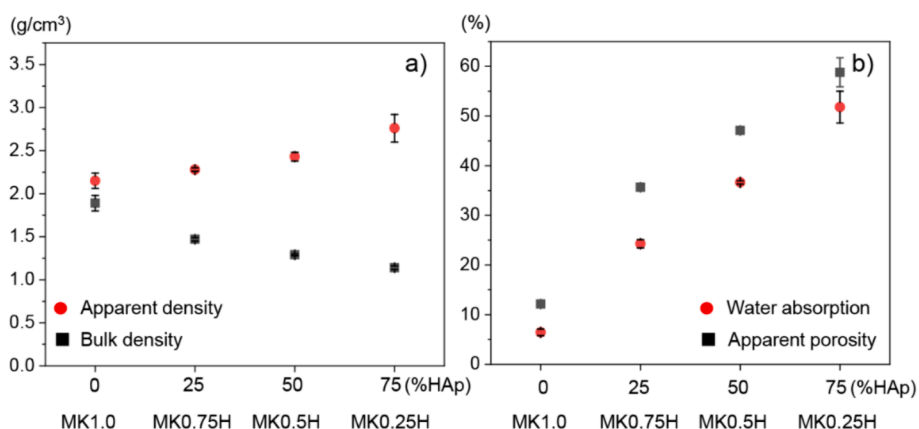


Fig. 2. (a) Relationships between bulk density/apparent density and HAp content, and (b) relationships between apparent porosity/water absorption and HAp content.

further contribute to porosity development during the curing process. Similar results were found by Rahmawati et al. (2022), Singh et al. (2021), Astariani et al. (2021), Kwek et al. (2021) and Chkala et al. (2024). Kwek et al. (2021) observed a decrease in geopolymer density with increasing alkaline activator-to-powder ratio. This density change is attributed to the influence of geopolymerization and curing

conditions. Their findings suggest that a high liquid content leads to a higher void volume within the samples. For bone mineral density, Meema and Meema (1978) reported that the normal range of bone density for women was between 0.96 g/cm³ and 1.39 g/cm³, while that for men was between 0.92 g/cm³ and 1.35 g/cm³, which overlap with the present range for metakaolin/HAp composites in Fig. 2(a).

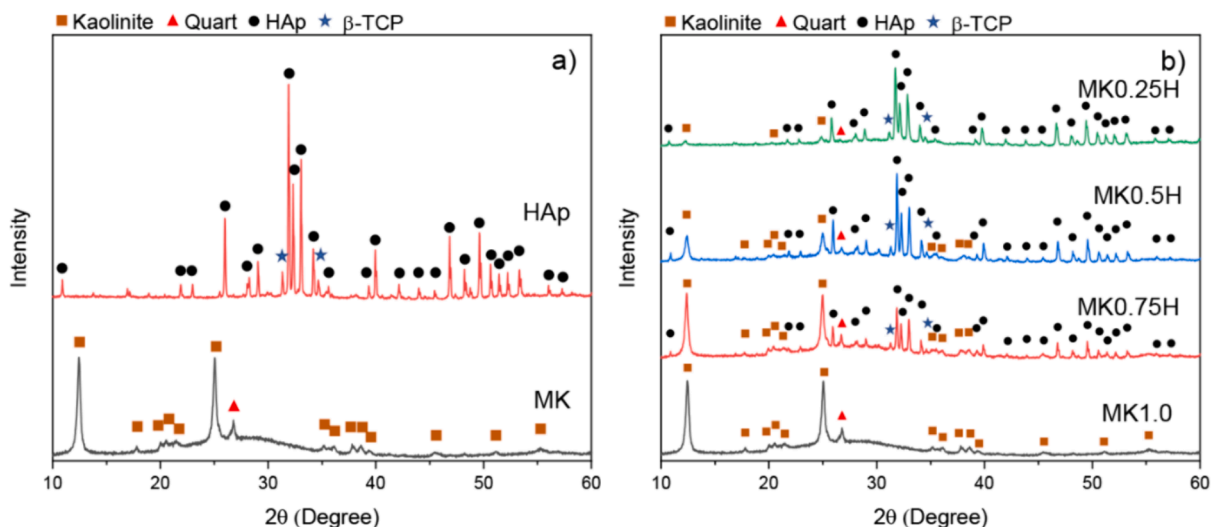


Fig. 3. XRD patterns for (a) MK and HAp powders and (b) MK1.0, MK0.75H, MK0.5H and MK0.25H samples.

The relationships between apparent porosity, water absorption and HAp content are shown in Fig. 2(b). From this figure, both the water absorption and apparent porosity increased with the HAp content, which may be induced by the increased difference between the bulk and apparent densities with higher HAp contents. The greater quantity of open pores with higher HAp contents may contribute to the increased water absorption and apparent porosity. Therefore, it is speculated that addition of HAp into the metakaolin/HAp composite can also lead to formation of more open pores. Generally, the open pores included in a material provide more open spaces for enhancing bone ingrowth. It has been reported that increased porosity is correlated with the degree and rate of bone ingrowth (Gawel et al., 2023).

Fig. 3(a) and (b) depict the XRD patterns for the MK and HAp powders and for MK1.0, MK0.75H, MK0.5H and MK0.25H samples, respectively. From Fig. 3(a), characteristic peaks of kaolinite (ICDD 00–001–0527) and quartz (ICDD 01–070–7345) were observed for MK powder. High intensity hydroxyapatite peaks (ICDD 09–0432) were observed coexisting with β -TCP (ICDD 09–0169) peaks for the HAp powder. From Fig. 3(b), characteristic peaks for MK and HAp are clearly observed in the post-cured samples. The peak intensity of HAp increased with its content. Geopolymerization did not affect the crystalline phases of MK and HAp.

SEM micrographs of sample surfaces are shown in Fig. 4. The surface morphology of MK1.0 and MK0.75H in Fig. 4(a) and (b) was nearly flat and dense. It becomes rough and the surface density decreased with greater HAp content (Fig. 4(c) and (d)). These density and surface appearance changes of the samples could be induced due to the presence of different content of HAp in the samples.

3.2. Cytotoxicity assay of the samples

A primary purpose of this experiment is to assess cellular cytotoxicity of MK/HAp composites towards osteoblast cells. Cell viability was assessed using a PrestoBlue assay after 24 h. The osteoblasts incubated on 30 and 90 mg of MK1.0, MK0.75H, MK0.5H and MK0.25H for 24 h were observed using optical microscopy. In Fig. 5, the osteoblasts maintain their normal shapes in all samples compared to the positive control, indicating no evidence of cytotoxicity.

Fig. 6 shows the average cell viability of the samples after incubation for 24 h. Cell viabilities of all samples were greater than 80 %. Furthermore, the average percentage of cell viability increased with HAp content. This increased cell viability demonstrates that HAp has potential to enhance the biocompatibility of MK/HAp composites towards osteoblast cells. Additionally, the sample quantity did not have a significant impact on biocompatibility of the MK/HAp composites. Cell viability remained unaffected by varying sample weights (30 mg and 90 mg) across all MK/HAp weight ratios. Catauro et al. (2020) conducted investigations on the cytotoxicity of a commercial MK geopolymer towards the NIH-3T3 mouse fibroblast cell line. Their study revealed that no toxic effects were observed on MK after 24 h of exposure. Interestingly, they reported that cell survival increased after 48 h of exposure, indicating a potential beneficial effect on cell viability over time.

3.3. In vitro bioactivity evaluation in simulated body fluid

3.3.1. Monolithic metakaolin MK1.0

Fig. 7(a) shows the surface morphology of a monolithic metakaolin (MK1.0) sample after immersion in SBF for 28 days. The surface morphology of the MK1.0 sample was flat and did not change appreciably after immersion in SBF for 28 days compared to that before immersion (Fig. 4(a)). The elemental composition obtained by EDS analysis on the surface of the MK1.0 sample immersed in SBF for 28 days is shown in Fig. 7(b). From the figure, the coexistence of silicon (Si), aluminum (Al), sodium (Na) was observed. Additionally, small peaks attributed to calcium (Ca) and phosphorus (P) were also observed in the EDS spectrum. The XRD pattern of the MK1.0 sample immersed for 28 days in SBF is shown in Fig. 7(c). The characteristic peaks of the MK1.0 sample immersed for 28 days were similar to those of the post-cured MK1.0 sample before immersion (Fig. 3(b)). No additional characteristic peaks were observed. Calcium and phosphorus detected on the surface of MK1.0 sample after immersion in SBF were possibly from residual SBF solution. The MK1.0 sample exhibited poor bioactivity due to a lack of calcium and phosphate ions, and it may have limited interaction with SBF due to the absence of pores (a very flat surface), both of which are essential for the formation of calcium phosphate apatite. Addition of hydroxyapatite into metakaolin is beneficial for

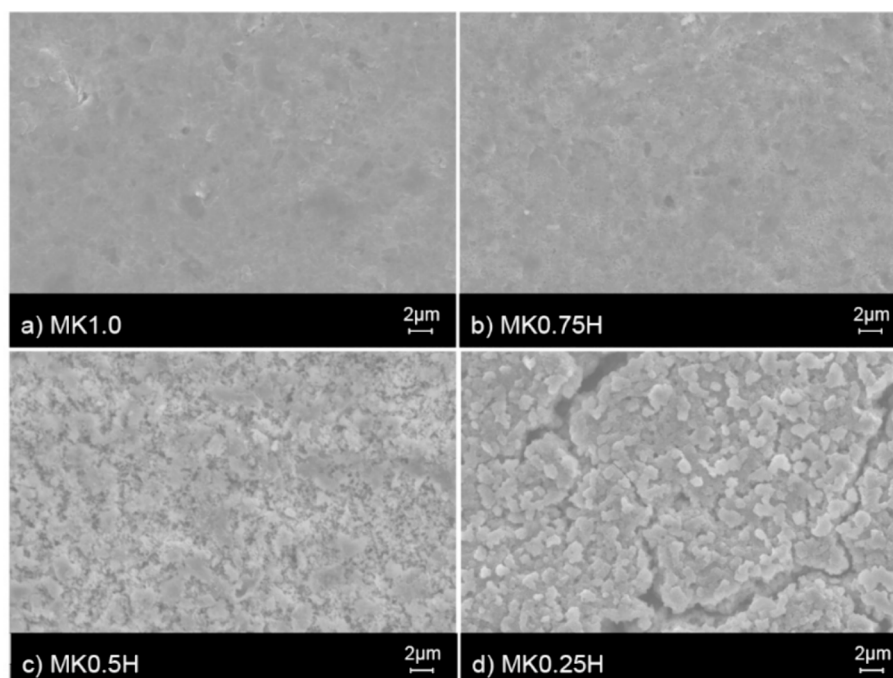


Fig. 4. Surface morphology of samples, (a) MK1.0, (b) MK0.75H, (c) MK0.5H and (d) MK0.25H.

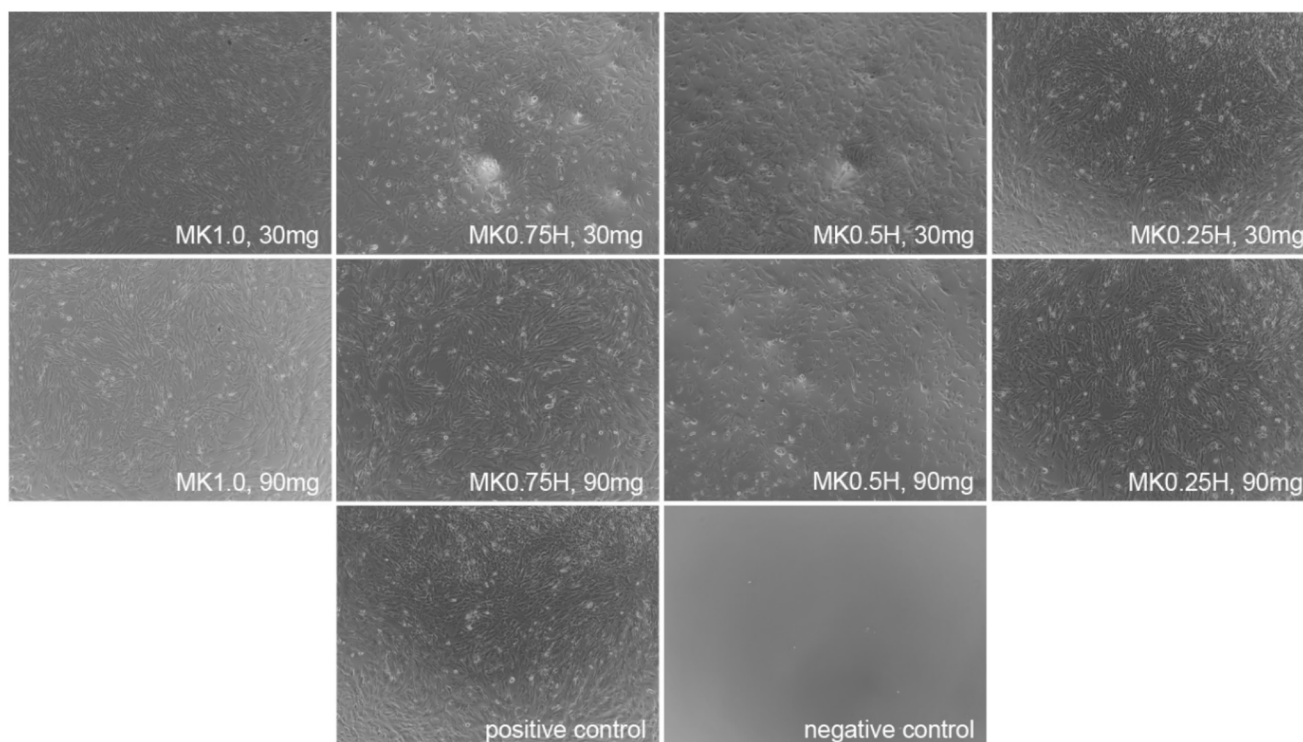


Fig. 5. Optical microscopy observations of osteoblasts incubated on 30 and 90 mg of MK1.0, MK0.75H, MK0.5H and MK0.25H composites.

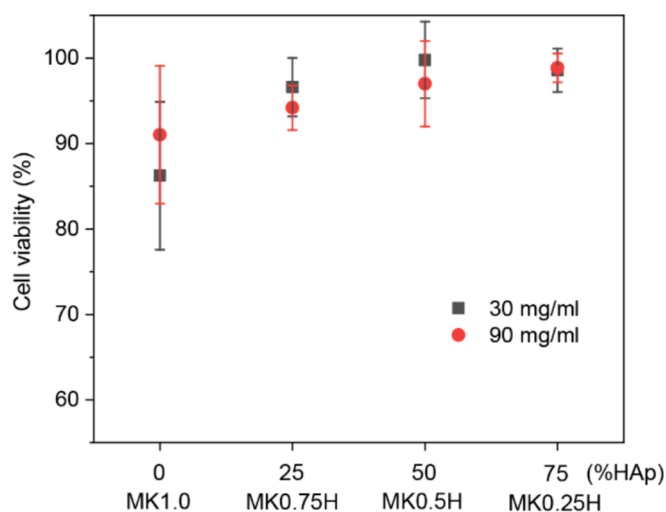


Fig. 6. Average percentage of cell viability of the MK/HAp samples (30 and 90 mg) after incubation tests for 24 h.

promoting nucleation sites for calcium phosphate apatite precipitation.

3.3.2. MK/HAp composites

MK0.75H, MK0.5H and MK0.25H composites were immersed in SBF for 3, 7, 14 and 28 days to investigate phase changes. Fig. 8 shows the surface morphology of the samples after immersion in SBF for 3 to 28 days. After 28 days, the surface of the MK0.25H sample (Fig. 8(l)) displayed comparatively dense spherical structures compared to the MK0.5H and MK0.75H samples (Fig. 8(k and j)). The MK0.25H sample changed its surface appearance faster than the MK0.5H and MK0.75H samples. Tiny spherical structures, approximately 1–2 μm in diameter, were observed on the MK0.25H surface after immersion in SBF for 3 days. A similar structure was clearly observed on the MK0.5H and

MK0.75H surfaces after 7 and 28 days of immersion, respectively. However, this spherical structure was not observed on the surface of MK geopolymer after immersion in SBF, as shown in Fig. 7(a). Similar bone-like apatite formation after immersion in SBF was reported by Gao et al. (2015), Taptimdee et al. (2020), Taptimdee et al. (2022) and Parau et al. (2023) where spherical structures of bone-like apatite were observed on the surfaces of their bone substitute after immersion in SBF for one to four weeks.

EDS spectra of the MK0.75H, MK0.5H and MK0.25H composites after immersion in SBF for 28 days are shown in Fig. 8(m-o). As seen from the figure, the same elements detected on the MK1.0 sample after immersion in SBF for 28 days (see Fig. 7(b)) were observed in the EDS spectra of MK0.75H, MK0.5H and MK0.25H composites with an additional magnesium (Mg) element. It was also found that the intensities of the Ca and P elements increased after immersion in SBF for the MK0.75H, MK0.5H and MK0.25H composites.

Variations of the Ca/P molar ratio after immersion in SBF for various periods are presented in Fig. 9. From this figure, the Ca/P molar ratio increased with the HAp content for the same immersion period. After 14 and 28 days of immersion, the Ca/P molar ratios for MK0.25H attained values of 1.60 and 1.66, respectively, which are close to that of stoichiometric HAp (1.67). It has been reported that the Ca/P molar ratio of biological (bone-like) apatite is either lower than or close to that of stoichiometric HAp (Eliaz and Metoki, 2017; Kuhn et al., 2008). The Ca/P ratios for cancellous and cortical bone have been reported as 1.47 and 1.64 for younger bone, respectively, and 1.52 and 1.66 for older bone, respectively (Kuhn et al., 2008). It was also found that a Ca/P molar ratio of 1.5 for MK0.5H after immersion in SBF for 28 days reached the range for cancellous and cortical bones. However, the Ca/P ratio for MK0.75H did not achieve those for human bone even after immersion in SBF for 28 days, which would result from calcium-deficiency in the calcium phosphate apatite layer. For biological apatite in bone tissue, similar structural formation, elemental composition and Ca/P molar ratio of calcium-phosphate apatite have been reported (Kim et al., 2004; Kim et al., 2005; Hadjipanteli et al., 2014).

From these results, addition of HAp in the MK/HAp composites could

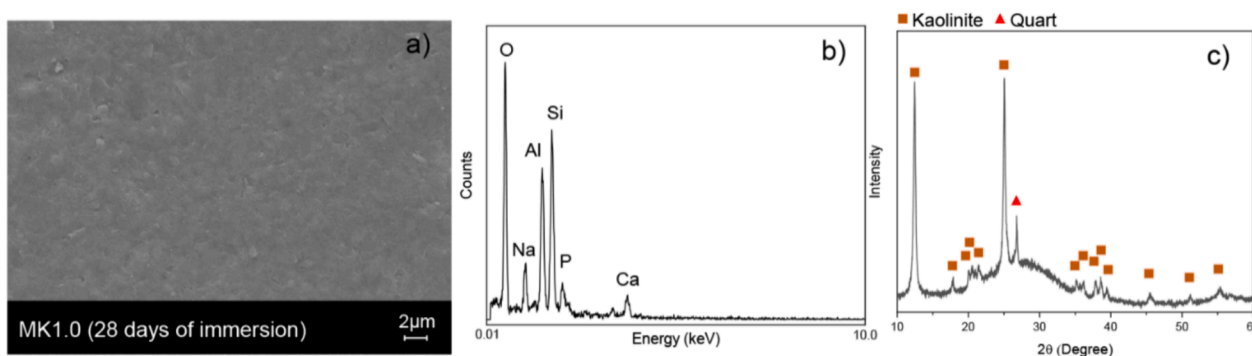


Fig. 7. (a) Surface morphology, (b) EDS spectrum and (c) XRD pattern of an MK1.0 sample after immersion in SBF for 28 days.

enhance bone-like apatite formation with spherical structures on surfaces during immersion in SBF. The density of the bone-like apatite structure increased with HAp content. The bone-like apatite structure grew and the Ca/P molar ratio of the bone-apatite layer increased after longer immersion periods. The Ca/P ratio was close to that of bone-like apatite for the MK/HAp composites with HAp contents greater than 50 % and after 28 days of immersion in SBF. *In vitro* bioactivity was studied on lignin/polycaprolactone nanofibers, fluorine-hydroxyapatite coatings and hydroxyapatite/tantalum composites (Wang et al., 2019; Cao et al., 2020; Cai et al., 2021). These studies support the present results that a dense spherical structure of bone-like apatite with a Ca/P molar ratio close to that of stoichiometric HAp is formed after immersion in SBF.

To confirm the phase transformation during SBF immersion, the phase composition of the MK/HAp composites before and after immersion for 14 and 28 days were investigated. Fig. 10 shows XRD patterns obtained on the surfaces of the MK0.75H, MK0.5H and MK0.25H composites before and after immersion in SBF. From this figure, the intensities of kaolinite, quartz and β -TCP peaks were reduced with increasing immersion periods, while the bases of hydroxyapatite peaks became broader for all the composites. These results indicate the progressive evolution of a bone-like apatite layer on the sample surfaces. This behavior was similar in all cases examined, however, there were variances in peak intensity for the same immersion period among the samples. The peak intensity of quartz vanished after 14 and 28 days of immersion for the MK0.5H and MK0.25H samples, respectively.

The results obtained from SEM observations, Ca/P molar ratio and XRD analysis indicated in the same direction that the addition of HAp to MK can enhance bone-like apatite formation and consequently improve bioactivity. Therefore, it can be concluded that bone-like apatite formation and surface morphology varied during *in vitro* bioactivity testing of MK/HAp composites depending on the period of immersion and HAp content. These results are consistent with those reported in the literature, where HAp was used to enhance the bioactivity in various bioactive materials such as titanium/hydroxyapatite (Bovand et al., 2019), Mg-hydroxyapatite (Mehdizade et al., 2023) and gelatin/hydroxyapatite (Zhang et al., 2020) composite materials. A bone-like apatite formation process can be proposed as the following. A HAp mixture provides nucleation sites for bone-like apatite precipitation. Then, hydroxyl (OH^-) and phosphate (PO_4^{3-}) groups on the surfaces of HAp carry negative charges, while calcium ions (Ca^{2+}) carry positive charges. HAp has a net negative charge that can attract positively charged calcium ions and other mineral ions, such as sodium (Na^+) or magnesium (Mg^{2+}) from the surrounding SBF solution. These mineral ions then nucleate and grow on the composite surfaces, forming bone-like apatite structures. The mechanism of bone-like apatite formation on synthetic hydroxyapatite using an *in vitro* assessment has been clearly explained by Kim et al. (2004) and (2005).

3.4. Effect of HAp content on compressive strength of the MK/HAp composites

The compressive strengths of the MK/HAp composites before and after immersion in SBF for 28 days are presented in Fig. 11. From this figure, the compressive strength of the MK/HAp composites significantly decreased with increasing HAp content regardless of immersion time in SBF, while immersion in SBF reduced the compressive strength. The results showed the compressive strengths before immersion in SBF were 58.2 and 14.3 MPa for the monolithic MK (MK1.0) and the MK0.25H composite with a 75 % HAp content, respectively. The reason for the reduction in strength with an increased HAp content involves the relationship between porosity and HAp content of the MK/HAp composites, as depicted in Fig. 11. As can be seen from this figure, the porosity formed in the MK/HAp composites increased with HAp content, which contributes to a reduced strength of the MK/HAp composite at greater HAp contents. However, from the viewpoint of strength of the monolithic HAp material, addition of MK into the HAp matrix would improve the strength of the MK/HAp composites.

From the results, it may be inferred that geopolymerization of metakaolin with an alkaline solution greatly impacts the formability and strength of the samples. Due to the reaction of silica and alumina species in metakaolin with the alkali activator solution, which promotes polycondensation events and development of a geopolymeric binder, an amorphous phase and a three-dimensional aluminosilicate network structure are formed (Albidah et al., 2021; Castillo et al., 2022). The compressive strength of the MK/HAp composites decreased due to an increase in porosity. Similar decrease in strength of MK/HAp composites with increasing HAp content has been reported by Tchakouté et al. (2018). They investigated the compressive strength of metakaolin-based geopolymers containing calcium phosphate compounds, such as hydroxyapatite, and found that it declines at metakaolin replacement levels above 2 % by weight. They reported that decreased compressive strength might be attributed to an excess PO_4 in the system, which weakens the specimen structure due to the presence of imbalanced (PO_4)³⁻ charges and thus negatively affects strength.

After immersion in SBF for 28 days, the compressive strengths were reduced regardless of HAp content, as shown in Fig. 11. The reduced compressive strengths after immersion in SBF were 39.8 MPa and 3.7 MPa for the monolithic MK (MK1.0) and the MK0.25H composite with 75 % HAp content, respectively. This decreased strength might be attributed to formation of micro-cracks inside the surface layer of samples during immersion in SBF. Such behavior would be due to water absorption combined with incomplete geopolymerization of the samples. Palomo et al. (1999) reported that dissolution of the soluble part of the material may occur during geopolymerization of metakaolin with an alkali activator solution. Most alkalis are fixed into the structure of the geopolymer, but some can remain soluble. These soluble alkalis can possibly dissolve, increasing the porosity of the specimen and, as a result, decrease its mechanical strength. The water resistance of

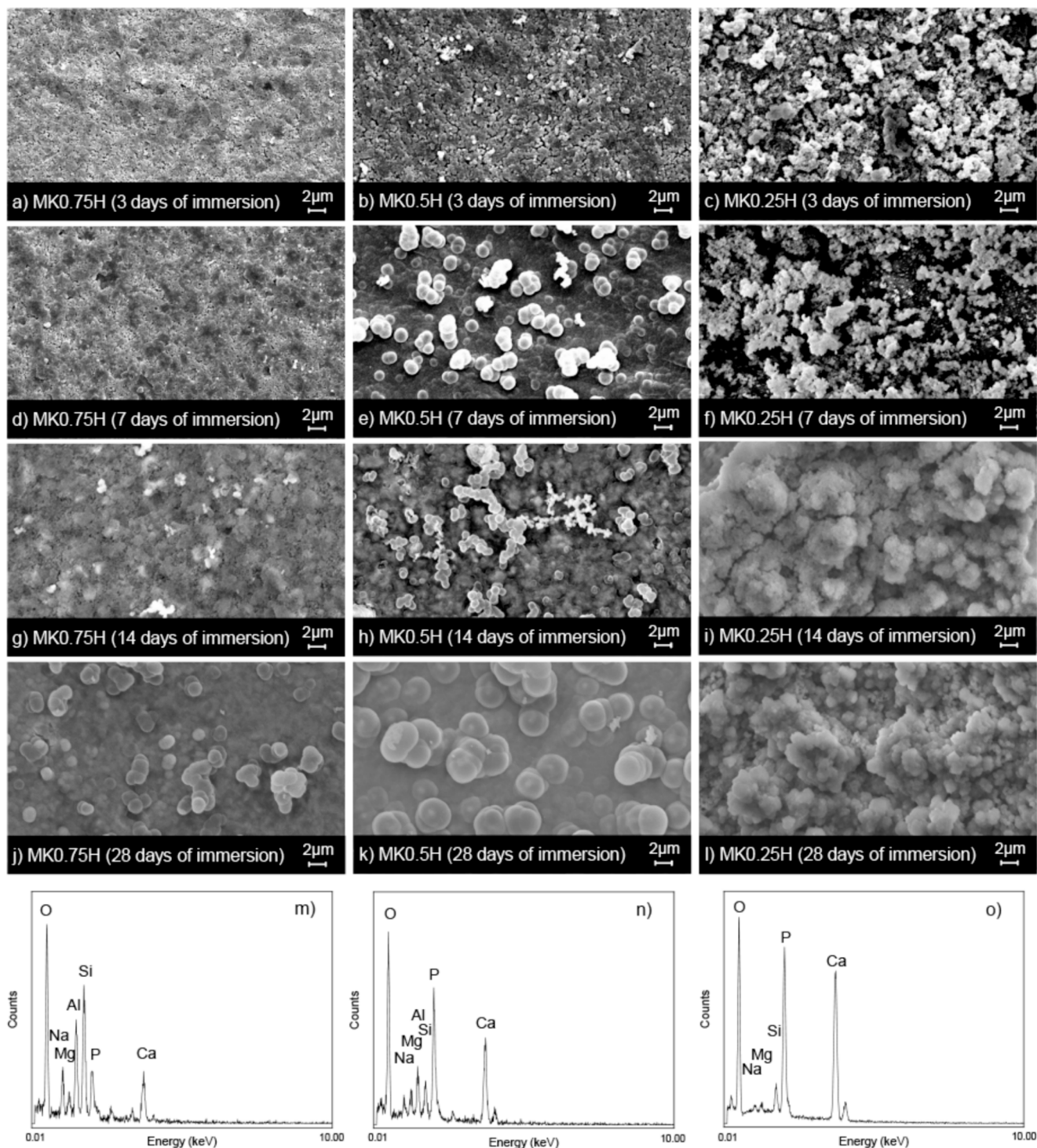


Fig. 8. Surface morphology of MK/HAp composites after immersion in SBF for 3, 7, 14 and 28 days (a-l) and EDS spectra of MK/HAp composites after immersion in SBF for 28 days (m-o).

geopolymer mortars made from granite waste as an aluminosilicate was investigated by Tchadjjié et al. (2016). They reported that formation of micro-cracks was observed in some types of geopolymer mortars within 48 h of immersion in water. Nikolić et al. (2013) also studied the durability of geopolymers in various aquatic environments. They reported that deterioration of the geopolymer structure in aquatic environments and leaching of the geopolymer structure reflect their stability. This phenomenon causes strength loss of geopolymers after immersion in distilled water, acid rain and sea water.

3.5. Suitable ratio of HAp content in MK/HAp composites

As discussed in the Introduction, improvement of strength and bioactivity due to variation of HAp content in MK/HAp composites has a competitive relationship. Therefore, for practical applications as a biomaterial, a suitable HAp content is important to clarify.

Based on the results presented in Fig. 9, the Ca/P molar ratios for the MK0.25H composite with a 75 % HAp content were 1.60 and 1.66 after immersion in SBF for 14 and 28 days, respectively. The Ca/P molar ratio

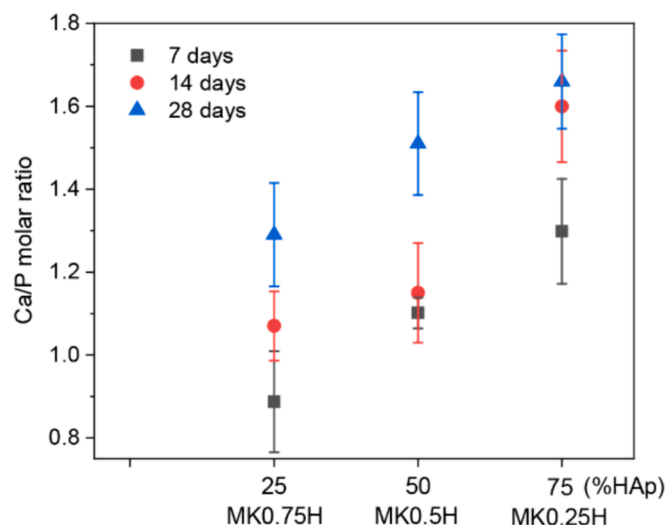


Fig. 9. Ca/P molar ratio of MK/HAp composites after immersion in SBF for 7, 14 and 28 days.

for the MK0.5H composite with a 50 % HAp content after immersion in SBF for 28 days attained a value of 1.5. These Ca/P molar ratios are equivalent to those for human bone. Therefore, HAp contents greater than 50 % are desirable for bioactivity.

Based on the results shown in Fig. 11, the porosity increased with HAp content. Porosity was higher than 35.6 % when the HAp content was greater than 25 %. Such a level of porosity would provide an acceptable environment to support bone regeneration. This range of porosity is consistent with the findings of other researchers who have developed biomaterials with various structures for bone tissue regeneration (Akbari and Khazaeinejad, 2023; Chen et al., 2017; Will et al., 2008). They reported scaffold porosity in the range between 30 and 60 %, which is close to that of natural (trabecular and cancellous) bone (40 to 90 %). This is sufficient for biomedical applications.

Based on the results shown in Fig. 11, the compressive strength decreases with increasing HAp content. Compressive strengths of human (trabecular and cancellous) bones are in the range of 2 to 15 MPa. A maximum strength of 15 MPa can be attained when the HAp content is between 25 and 50 %. However, human bone properties exhibit significant variations based on age, anatomic location and metabolic location (Oftadeh et al., 2015; Hussein et al., 2023). Therefore, a HAp content 50 % or higher can be selected to match specific human bones.

Since the bioactivity and bone regeneration behavior is sufficient for use as biomaterials when the HAp content is 50 % or higher, a suitable HAp content can be selected for bone substitute materials to match the strength of specific human bones. However, extensive studies on the

alkaline phosphatase (ALP) activity and the *in vitro* and *in vivo* biodegradability of this composite are required. These studies would provide valuable insights into their ability to support early bone formation and their long-term performance as bone substitutes.

4. Conclusions

Metakaolin/hydroxyapatite (MK/HAp) composites with various HAp contents for use as synthetic bone substitute materials were fabricated to investigate the effects of HAp content on *in vitro* properties including cytotoxicity and bioactivity as well as physical and mechanical characteristics. The primary conclusions obtained from the present study are as follows.

1. With increasing HAp content in the MK/HAp composites, their bulk density decreased, and porosity and percentage of water absorption increased.
2. The cytotoxicity of the MK/HAp composites was investigated using a PrestoBlue assay, which confirmed that the MK/HAp composites had acceptable osteoblast cell compatibility. The cell viability was approximately 80 % for the metakaolin geopolymer and increased with the HAp content in the MK/HAp composites.
3. *In vitro* bioactivity of the MK/HAp composites was investigated by immersing the samples in a simulated body fluid (SBF). Bone-like apatite formation on the surface of MK/HAp composites occurred more rapidly with increased HAp content, showing that HAp

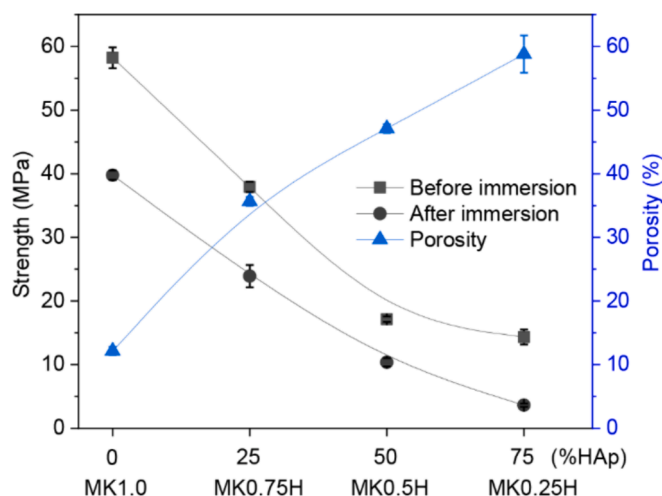


Fig. 11. Relationships between compressive strength and percentage of HAp content for MK/HAp composites before and after immersion in SBF for 28 days and between porosity and HAp content.

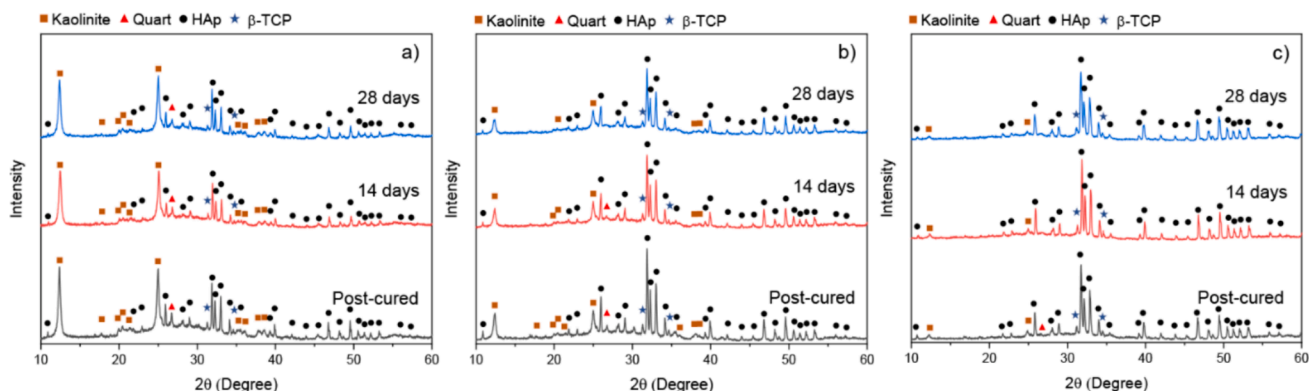


Fig. 10. XRD patterns of (a) MK0.75H, (b) MK0.5H and (c) MK0.25H composites before and after immersion in SBF for 14 and 28 days.

addition enhances bioactivity of the composites. This did not happen on the surfaces of MK geopolymers.

- The compressive strength of MK/HAp composites decreased with increasing HAp content mainly due to the reduced amount of silica and alumina in the system and increased porosity. After immersion in SBF, the compressive strengths of all samples decreased due to dissolved solutes which increased sample porosity.
- Selection of a suitable ratio of HAp content for balancing compressive strength and bioactivity is important. The bioactivity and bone regeneration behaviour can be sufficient for its application as a biomaterial when the HAp content is higher than 50 %. Therefore, a suitable HAp content, greater than 50 %, is necessary when formulating a bone substitute material to match the strengths of specific human bones.

CRediT authorship contribution statement

Nattaphon Twinprai: Writing – original draft, Validation, Methodology, Investigation, Formal analysis. **Ratchawoot Sutthi:** Visualization, Validation, Investigation, Formal analysis. **Piboon Ngaonee:** Validation, Methodology, Investigation, Formal analysis. **Patamaporn Chaikool:** Validation, Methodology, Investigation, Formal analysis. **Tularat Sookto:** Methodology, Formal analysis. **Prin Twinprai:** Validation, Methodology. **Yoshiharu Mutoh:** Writing – review & editing, Validation, Supervision. **Prinya Chindaprasirt:** Writing – review & editing, Supervision. **Teerawat Laonapakul:** Writing – original draft, Visualization, Validation, Methodology, Investigation, Funding acquisition, Formal analysis, Data curation, Conceptualization.

Declaration of competing interest

The authors declare that they have no known competing financial interests or personal relationships that could have appeared to influence the work reported in this paper.

Acknowledgements

This research was supported by the Fundamental Fund of Khon Kaen University through the National Science, Research and Innovation Fund (NSRF) of Thailand.

References

- Akbari, S., Khazaeinejad, P., 2023. Geometrical and mechanical analysis of polylactic acid and polyvinylidene fluoride scaffolds for bone tissue engineering. *Eng. Comput.* 39, 4153–4165. <https://doi.org/10.1007/s00366-023-01902-y>.
- Albidah, A., Alghannam, M., Abbas, H., Almusallam, T., Al-Salloum, Y., 2021. Characteristics of metakaolin-based geopolymer concrete for different mix design parameters. *J. Mater. Res. Technol.* 10, 84–98. <https://doi.org/10.1016/j.jmrt.2020.11.104>.
- Alvarado, C., Alfaro, A., Cisneros, M., Alvarado-Quintana, H., 2023. Preparation and characterization of hydroxyapatite obtained from bovine bones. *Proceedings of the 21st LACCEL International Multi-Conference for Engineering, Education and Technology: Leadership in Education and Innovation in Engineering in the Framework of Global Transformations: Integration and Alliances for Integral Development*, LACCEL, 10.18687/LACCEL2023.1.1.590.
- Astariani, N.K., Salain, I.M.A.K., Sutarja, I.N., Widiarsa, I.B.R., 2021. E effect alkaline activator ratio on porosity geopolymer binder based uameanyar slate stone powder. *International Journal of Engineering and Emerging Technology*. 6, 1–5. Available at: Date accessed: 22 May. 2024 ISSN 2579-5988.
- ASTM C109/C109M, 2021. Standard Test Method for Compressive Strength of Hydraulic Cement Mortars (Using 2-in. or [50-mm] Cube Specimens). ASTM International. West Conshohocken: PA.
- ASTM C373-88, 2006. Standard Test Method for Water Absorption, Bulk Density, Apparent Porosity, and Apparent Specific Gravity of Fired Whiteware Products. ASTM International. West Conshohocken: PA.
- Bovand, D., Allazadeh, M.R., Rasouli, S., Khodadad, E., Borhani, E., 2019. Studying the effect of hydroxyapatite particles in osteoconductivity of Ti-HA bioceramic. *J. Aust. Ceram. Soc.* 55, 395–403. <https://doi.org/10.1007/s41779-018-0247-7>.
- Brown, P.W., 2001. Calcium phosphates in biomedical engineering. *Encyclopedia of Materials: Science and Technology* 893–897. <https://doi.org/10.1016/B0-08-043152-6/00170-4>.

- Cai, C., Wang, X., Li, B., Dong, K., Shen, Y., Li, Z., Shen, L., 2021. Fabrication of hydroxyapatite/tantalum composites by pressureless sintering in different atmosphere. *ACS Omega* 6, 12831–12840. <https://doi.org/10.1021/acsomega.1c01205>.
- Cao, J., Lian, R., Jiang, X., Liu, X., 2020. Formation of porous apatite layer after immersion in SBF of fluorine-hydroxyapatite coatings by pulsed laser deposition improved in vitro cell proliferation. *ACS Appl. Bio Mater.* 3, 3698–3706. <https://doi.org/10.1021/acsbm.0c00328>.
- Castillo, H., Collado, H., Drogue, T., Vesely, M., Garrido, P., Palma, S., 2022. State of the art of geopolymers: A review. *E-Polymers* 22, 108–124. <https://doi.org/10.1515/epoly-2022-0015>.
- Catauro, M., Bollino, F., Papale, F., Lamanna, G., 2014. Investigation of the sample preparation and curing treatment effects on mechanical properties and bioactivity of silica rich metakaolin geopolymer. *Mater. Sci. Eng.* 36, 20–24. <https://doi.org/10.1016/j.msec.2013.11.026>.
- Catauro, M., Dal Poggetto, G., Sgarlata, C., Cipriotti, S.V., Pacifico, S., Leonelli, C., 2020. Thermal and microbiological performance of metakaolin-based geopolymers cement with waste glass. *Appl. Clay Sci.* 197, 105763. <https://doi.org/10.1016/j.clay.2020.105763>.
- Chen, Y., Frith, J.E., Dehghan-Manshadi, A., Attar, H., Kent, D., Soro, N.D.M., Bermingham, M.J., Dargusch, M.S., 2017. Mechanical properties and biocompatibility of porous titanium scaffolds for bone tissue engineering. *J. Mech. Behav. Biomed. Mater.* 75, 169–174. <https://doi.org/10.1016/j.jmbm.2017.07.015>.
- Chkala, H., Kirm, I., Ighir, S., Ourmiche, A., Chigr, M., El Mansouri, N.E., 2024. Preparation and characterization of eco-friendly composite based on geopolymer and reinforced with date palm fiber. *Arab. J. Chem.* 17, 105510. <https://doi.org/10.1016/j.arabjc.2023.105510>.
- de Andrade, R., Paim, T.C., Bertaco, I., Naasani, L.S., Buchner, S., Kovárík, T., Hájek, J., Wink, M.R., 2023. Hierarchically porous bioceramics based on geopolymer-hydroxyapatite composite as a novel biomaterial: Structure, mechanical properties and biocompatibility evaluation. *Appl. Mater. Today*. 33, 101875. <https://doi.org/10.1016/j.apmt.2023.101875>.
- Du, X., Pang, D., Zhao, Y., Hou, Z., Wang, H., Cheng, Y., 2022. Investigation into the Adsorption of CO₂, N₂ and CH₄ on Kaolinite Clay. *Arab. J. Chem.* 15, 103665. <https://doi.org/10.1016/j.arabjc.2021.103665>.
- Eliaz, N., Metoki, N., 2017. Calcium phosphate bioceramics: a review of their history, structure, properties, coating technologies and biomedical applications. *Materials*. 10, 334. <https://doi.org/10.3390/ma10040334>.
- Feng, P., Zhao, R., Tang, W., Yang, F., Tian, H., Peng, S., Pan, H., Shuai, C., 2023. Structural and functional adaptive artificial bone: materials, fabrications, and properties. *Adv. Funct. Mater.* 33, 2214726. <https://doi.org/10.1002/adfm.202214726>.
- Gao, C., Wei, P., Feng, P., Xiao, T., Shuai, C., Peng, S., 2015. Nano SiO₂ and MgO improve the properties of porous β -TCP scaffolds via advanced manufacturing technology. *Int. J. Mol. Sci.* 16, 6818–6830. <https://doi.org/10.3390/ijms16046818>.
- Gawel, J., Milan, J., Żebrowski, J., Ploch, D., Stefaniuk, I., Kus-Liśkiewicz, M., 2023. Biomaterial composed of chitosan, riboflavin, and hydroxyapatite for bone tissue regeneration. *Sci. Rep.* 13, 17004. <https://doi.org/10.1038/s41598-023-44225-0>.
- Hadjipanteli, A., Kourkoumelis, N., Speller, R., 2014. Evaluation of CT-DEA performance on Ca/P ratio assessment in bone apatite using EDX. *X-Ray Spectrom.* 43, 286–291. <https://doi.org/10.1002/xrs.2551>.
- Herford, A.S., Stoffella, E., Stanford, C.M., 2014. Bone grafts and bone substitute materials. In: *Principles and Practice of Single Implant and Restorations*. Elsevier Inc., pp. 75–86. [10.1016/B978-1-4557-4476-3.00005-6](https://doi.org/10.1016/B978-1-4557-4476-3.00005-6).
- Hussein, R., Landon, Y., Araujo, A.C., 2023. Bone properties -: A review for drilling application. *COBEF*. <https://hal.science/hal-04002794>.
- Jurgelane, I., Buss, A., Putnina, M., Loca, D., Locs, J., 2021. Effect of sintering temperature on sorption properties and compressive strength of calcium phosphate ceramic granules. *Mater. Lett.* 282, 128858. <https://doi.org/10.1016/j.matlet.2020.128858>.
- Kanis, J.A., 2007. Assessment of osteoporosis at the primary health care level, WHO Collaborating Centre for Metabolic Bone Diseases, University of Sheffield Medical School: Printed by the University of Sheffield, p. 6.
- Kim, H.M., Himeno, T., Kawashita, M., Kokubo, T., Nakamura, T., 2004. The mechanism of biomineralization of bone-like apatite on synthetic hydroxyapatite: an in vitro assessment. *J. r. Soc. Interface*. 1, 17–22. <https://doi.org/10.1098/rsif.2004.0003>.
- Kim, H.M., Himeno, T., Kokubo, T., Nakamura, T., 2005. Process and kinetics of bonelike apatite formation on sintered hydroxyapatite in a simulated body fluid. *Biomaterials* 26, 4366–4373. <https://doi.org/10.1016/j.biomaterials.2004.11.022>.
- Kim, C., Lee, J.W., Heo, J.H., Park, C., Kim, D.H., Yi, G.S., Kang, H.C., Jung, H.S., Shin, H., Lee, J.H., 2022. Natural bone-mimicking nanopore-incorporated hydroxyapatite scaffolds for enhanced bone tissue regeneration. *Biomaterials Research*. 26, 1–13. <https://doi.org/10.1186/s40824-022-00253-x>.
- Kokubo, T., Takadama, H., 2006. How useful is SBF in predicting in vivo bone bioactivity? *Biomaterials* 27, 2907–2915. <https://doi.org/10.1016/j.biomaterials.2006.01.017>.
- Kuhn, L.T., Grynypas, M.D., Rey, C.C., Wu, Y., Ackerman, J.L., Glimcher, M.J., 2008. A comparison of the physical and chemical differences between cancellous and cortical bovine bone mineral at two ages. *Calcif. Tissue Int.* 83, 146–154. <https://doi.org/10.1007/s00223-008-9164-z>.
- Kwek, S.Y., Awang, H., Cheah, C.B., 2021. Influence of liquid-to-solid and alkaline activator (sodium silicate to sodium hydroxide) ratios on fresh and hardened properties of alkali-activated palm oil fuel ash geopolymer. *Materials* 14, 4253. <https://doi.org/10.3390/ma14154253>.

- Lahoti, M., Tan, K.H., Yang, E.H., 2019. A critical review of geopolymer properties for structural fire-resistance applications. *Constr. Build. Mater.* 221, 514–526. <https://doi.org/10.1016/j.conbuildmat.2019.06.076>.
- Laonapakul, T., Sutthi, R., Chaikool, P., Talangkun, S., Boonma, A., Chindaprasirt, P., 2021. Calcium phosphate powders synthesized from CaCO₃ and CaO of natural origin using mechanical activation in different media combined with solid-state interaction. *Mater. Sci. Eng.* 118, 111333 <https://doi.org/10.1016/j.msec.2020.111333>.
- Maruoka, L.M., Pinheiro, I.F., Freitas, H.S., Nobre, F.X., Scalvi, L.V., 2023. Effect of thermal annealing on kaolin from the Amazon region, aiming at the production of geopolymer. *J. Mater. Res. Technol.* 25, 2471–2485. <https://doi.org/10.1016/j.jmrt.2023.06.105>.
- Mataalkah, F., Ababneh, A., Aqel, R., 2023. Synthesis of calcined kaolin-based geopolymer foam: Assessment of mechanical properties, thermal insulation, and elevated temperature stability. *Ceram. Int.* 49, 9967–9977. <https://doi.org/10.1016/j.ceramint.2022.11.174>.
- Meema, H.E., Meema, S., 1978. Compact bone mineral density of the normal human radius. *Acta. Radiol.* 17, 342–352. <https://doi.org/10.3109/02841867809127938>.
- Mehdizade, M., Eivani, A.R., Asgari, H., Naghshin, Y., Jafarian, H.R., 2023. Assessment of microstructure, biocompatibility and in-vitro biodegradation of a biomedical Mg-Hydroxyapatite composite for bone tissue engineering. *J. Mater. Res. Technol.* 27, 852–875. <https://doi.org/10.1016/j.jmrt.2023.09.245>.
- Metzner, F., Neupetsch, C., Fischer, J.P., Drossel, W.G., Heyde, C.E., Schleifenbaum, S., 2021. Influence of osteoporosis on the compressive properties of femoral cancellous bone and its dependence on various density parameters. *Sci. Rep.* 11, 13284. <https://doi.org/10.1038/s41598-021-92685-z>.
- Misch, C.E., Qu, Z., Bidez, M.W., 1999. Mechanical properties of trabecular bone in the human mandible: implications for dental implant treatment planning and surgical placement. *J. Oral Maxillofac. Surg.* 57, 700–706. [https://doi.org/10.1016/S0278-2391\(99\)90437-8](https://doi.org/10.1016/S0278-2391(99)90437-8).
- Moya, J.S., Cabal, B., Lopez-Esteban, S., Bartolomé, J.F., Sanz, J., 2024. Significance of the formation of pentahedral aluminum in the reactivity of calcined kaolin/metakaolin and its applications. *Ceram. Int.* 50, 1329–1340. <https://doi.org/10.1016/j.ceramint.2023.10.304>.
- Müller, A.S., Janjić, K., Shokoohi-Tabrizi, H., Oberoi, G., Moritz, A., Agis, H., 2020. The response of periodontal cells to kaolinite. *Clin. Oral Investig.* 24, 1205–1215. <https://doi.org/10.1007/s00784-019-02984-z>.
- Nikolić, I., Zejak, R., Janković-Častvan, I., Karanović, L., Radmilović, V., Radmilović, V. R., 2013. Influence of alkali cation on the mechanical properties and durability of fly ash based geopolymers. *Acta Chim. Slov.* 60 (636), 43. <https://acsjournal.eu/index.php/ACSi/article/view/100>.
- Obada, D.O., Osseni, S.A., Sina, H., Salami, K.A., Oyedeji, A.N., Dodoo-Arhin, D., Bansod, N.D., Csaki, S., Atta, A.Y., Fasanya, O.O., Sowunmi, A.R., 2021. Fabrication of novel kaolin-reinforced hydroxyapatite scaffolds with robust compressive strengths for bone regeneration. *Appl. Clay Sci.* 215, 106298 <https://doi.org/10.1016/j.clay.2021.106298>.
- Oftadeh, R., Perez-Viloria, M., Villa-Camacho, J.C., Vaziri, A., Nazarian, A., 2015. Biomechanics and mechanobiology of trabecular bone: a review. *J. Biomech. Eng.* 137, 010802 <https://doi.org/10.1115/1.4029176>.
- Palomo, A., Blanco-Varela, M.T., Granizo, M.L., Puertas, F., Vazquez, T., Grutzeck, M.W., 1999. Chemical stability of cementitious materials based on metakaolin. *Cem. Concr. Res.* 29, 997–1004. [https://doi.org/10.1016/S0008-8846\(99\)00074-5](https://doi.org/10.1016/S0008-8846(99)00074-5).
- Pangdaeng, S., Sata, V., Chindaprasirt, P., 2018. Effect of sodium hydroxide concentration and sodium silicate to sodium hydroxide ratio on properties of calcined kaolin-white portland cement geopolymer. *Int. J. GEOMATE.* 14, 121–128. <https://doi.org/10.21660/2018.46.mat40>.
- Parau, A.C., Dinu, M., Vitelaru, C., Cotrut, C.M., Vranceanu, D.M., Vladescu, A., 2023. Quaternary ZrCuCa-based thin films metallic glasses deposited by cathodic arc deposition. *Arab. J. Chem.* 16, 105312 <https://doi.org/10.1016/j.arabjc.2023.105312>.
- Rahmawati, C., Aprilia, S., Saidi, T., Aulia, T.B., Amin, A., Ahmad, J., Isleem, H.F., 2022. Mechanical properties and fracture parameters of geopolymers based on cellulose nanocrystals from *Typha sp.* fibers. *Case. Stud. Constr. Mater.* 17, e01498.
- Sakka, S., Bouaziz, J., Ayed, F.B., 2013. Mechanical properties of biomaterials based on calcium phosphates and bioinert oxides for applications in biomedicine. *INTECH* 23–50. <https://doi.org/10.5772/53088>.
- Shuai, C., Yang, W., Feng, P., Peng, S., Pan, H., 2021. Accelerated degradation of HAP/PLLA bone scaffold by PGA blending facilitates bioactivity and osteoconductivity. *Bioact. Mater.* 6, 490–502. <https://doi.org/10.1016/j.bioactmat.2020.09.001>.
- Shuai, C., Peng, B., Feng, P., Yu, L., Lai, R., Min, A., 2022. In situ synthesis of hydroxyapatite nanorods on graphene oxide nanosheets and their reinforcement in biopolymer scaffold. *J. Adv. Res.* 35, 13–24. <https://doi.org/10.1016/j.jare.2021.03.009>.
- Singh, N.S., Thokchom, S., Debbarma, R., 2021. Properties of fly ash and rice husk ash blended geopolymer with sodium aluminate as activator solution. *Eng. Appl. Sci. Res.* 48, 92–101. <https://ph01.tci-thaijo.org/index.php/easr/article/view/240316>.
- Sutthi, R., Kaewwinud, N., Chindaprasirt, P., Mutoh, Y., Laonapakul, T., 2018. Effect of curing temperature and time on the mechanical properties of hydroxyapatite/calcined kaolin. *Sci. Asia.* 44, 397. <https://doi.org/10.2306/sciencasia1513-1874.2018.44.397>.
- Taptimdee, W., Chindaprasirt, P., Otsuka, Y., Mutoh, Y., Laonapakul, T., 2020. Strength and bioactivity of hydroxyapatite/white portland cement (HAP/WPC) under Simulated Body Fluid (SBF) solution. *Mater. Sci. Forum* 975, 88–93. <https://doi.org/10.4028/www.scientific.net/MSF.975.88>.
- Taptimdee, W., Jantasang, A., Chindaprasirt, P., Otsuka, Y., Mutoh, Y., Laonapakul, T., 2022. Effect of an in vitro environment on compressive strength and apatite formation of white Portland cement. *Engineering & Applied Science Research* 49, 181–188. <https://doi.org/10.14456/easr.2022.20>.
- Tchadjé, L.N., Djobo, J.N.Y., Ranjbar, N., Tchakouté, H.K., Kenne, B.D., Elimbi, A., Njopwouo, D., 2016. Potential of using granite waste as raw material for geopolymer synthesis. *Ceram. Int.* 42, 3046–3055. <https://doi.org/10.1016/j.ceramint.2015.10.091>.
- Tchakouté, H.K., Fotio, D., Rüscher, C.H., Kamseu, E., Djobo, J.N., Bignozzi, M.C., Leonelli, C., 2018. The effects of synthesized calcium phosphate compounds on the mechanical and microstructural properties of metakaolin-based geopolymer cements. *Constr. Build. Mater.* 163, 776–792. <https://doi.org/10.1016/j.conbuildmat.2017.12.162>.
- Wang, Y.S., Alrefaei, Y., Dai, J.G., 2019b. Silico-aluminophosphate and alkali-aluminosilicate geopolymers: A comparative review. *Front. Mater.* 6, 106. <https://doi.org/10.3389/fmats.2019.00106>.
- Wang, D., Jang, J., Kim, K., Kim, J., Park, C.B., 2019a. “Tree to bone”: lignin/polycaprolactone nanofibers for hydroxyapatite biomineralization. *Biomacromolecules* 20, 2684–2693. <https://doi.org/10.1021/acs.biomac.9b00451>.
- Will, J., Melcher, R., Treul, C., Travitzky, N., Kneser, U., Polykandriotis, E., Horch, R., Greil, P., 2008. Porous ceramic bone scaffolds for vascularized bone tissue regeneration. *J. Mater. Sci. Mater. Med.* 19, 2781–2790. <https://doi.org/10.1007/s10856-007-3346-5>.
- Zhang, Z., Li, K., Zhou, W., Gu, J.G., Liu, Y., Han, C.C., Xu, S., 2020. Factors influencing the interactions in gelatin/hydroxyapatite hybrid materials. *Front. Chem.* 8, 489. <https://doi.org/10.3389/fchem.2020.00489>.